

# Dual Role of MoS<sub>2</sub> Quantum Dots in a Cross-Dehydrogenative Coupling Reaction

Komal Jaiswal, Yarabahally R. Girish, Pradipta Behera, and Mrinmoy De\*

Cite This: *ACS Org. Inorg. Au* 2022, 2, 205–213

Read Online

ACCESS |



Metrics &amp; More



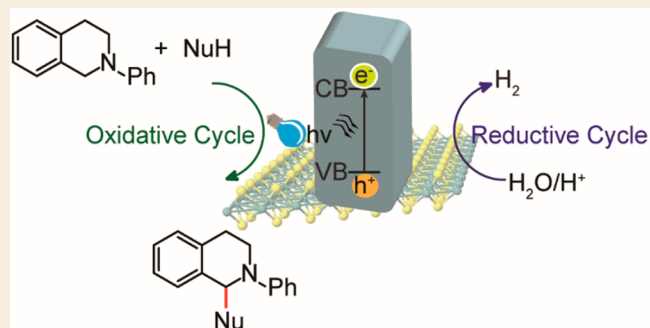
Article Recommendations



Supporting Information

**ABSTRACT:** Modern day research focuses on the development of greener and eco-friendlier protocols to fabricate biologically relevant targets with minimal waste generation. C–C bond formation reactions are of prime importance in this regard. In a typical photocatalytic hydrogen evolution reaction, three components are used, viz, catalyst, photosensitizer, and sacrificial amine donor. Among these, the photosensitizer and sacrificial amine donors are wasted at the end of the reaction. Considering these drawbacks, in this work, we have developed a methodology targeted at the utilization of sacrificial amine donors for C–H functionalization with MoS<sub>2</sub> quantum dots (QDs) as the catalyst as well as the photosensitizer. QDs indeed emerged to be an active participant in the heterogeneous electron transfer process. This concept opens up new possibilities in the field of nanomaterial-based photomediated organic transformations without the aid of any external photosensitizers via a clean and sustainable protocol with no side product.

**KEYWORDS:** quantum dots, transition metal dichalcogenides, cross-dehydrogenative coupling, photoredox, heterogeneous electron transfer



## INTRODUCTION

Quantum dots (QDs) are nanomaterials having a diameter in the range of 2–10 nm and an enhanced surface-to-volume ratio that generates a greater number of active sites. They display a wide range of absorption and emission depending on their size<sup>1–3</sup> and surface property,<sup>4–7</sup> which is a consequence of the direct band gap<sup>8,9</sup> in these materials, contrary to their bulk counterparts. The most unique feature of these materials is the ability to be confined in a small space, often referred to as quantum confinement.<sup>10,11</sup> This results in the quantization of energy levels. In this regard, QDs are more closely related to atoms than bulk materials and are popularly known as “artificial atoms”.<sup>12</sup> The band gap increases with a decrease in the size of the nanomaterial.<sup>13</sup> Commonly known QDs are those of CdS and CdSe. However, these materials are associated with an inherent toxicity.<sup>14,15</sup> Various reports discuss the catalytic applications of materials like CdSe or InP/ZnS QDs.<sup>16,17</sup> Nanostructures such as QDs are favored over the bulk counterparts as one can exploit the properties of lower dimensions such as a larger surface area in catalytic and other relevant applications.<sup>13</sup>

Transition metal dichalcogenides (TMDs) are binary compounds of the type MX<sub>2</sub> with M being a transition metal from groups 4–6 while X is a chalcogen atom (S, Se, Te). Owing to the weak van der Waals forces that bind the layers, the earth-abundant bulk forms can be converted to lower-dimensional counterparts such as QDs and nanosheets, which

can be modified in terms of composition, morphology, etc. to obtain the desired properties. Being heterogeneous participants in electron-transfer processes,<sup>18</sup> these solve the issue of lack of recyclability. TMD QDs have exclusive semiconducting properties, dictated by band gap, functionalization, size, structure, etc. Owing to the easiness of preparation from molybdenite precursors, MoS<sub>2</sub> continues to be the most suitable TMD for various catalytic,<sup>19,20</sup> electronics,<sup>21</sup> biological,<sup>22</sup> and energy-related<sup>23,24</sup> applications. Atomic defects confer additional chemical and optoelectronic properties which can also alter the catalytic activity.<sup>25</sup> Despite the aforementioned advantages, until now, the catalytic activity of such materials has not been explored extensively.

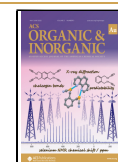
MoS<sub>2</sub> QDs can be prepared with a bottom-up or a top-down approach. In the second method, organic solvent(s) such as *N,N*-dimethylformamide (DMF) are used typically.<sup>26</sup> Using an organic solvent comes with its own disadvantages such as formation of carbon dots at high temperature or pressure. Thus, protocols that rely on the use of water as the solvent are advantageous. Synthesis of MoS<sub>2</sub> QDs has recently drawn

**Received:** October 29, 2021

**Revised:** December 6, 2021

**Accepted:** December 6, 2021

**Published:** February 22, 2022



significant attention as these have a high extinction coefficient in the visible region, hence they can harvest light efficiently. Unlike the conventional organic dyes or commonly used transition metal complexes, these are more stable in the presence of radiation. They have been used extensively in the hydrogen evolution reaction (HER),<sup>27–30</sup> oxygen evolution reaction (OER),<sup>31</sup> bioimaging,<sup>32–36</sup> degradation of dye,<sup>37</sup> sensing,<sup>38–41</sup> and therapeutic applications.<sup>42–44</sup>

Coupling reactions have emerged as crucial methodologies for C–C bond formation.<sup>45</sup> Cross-coupling reactions came into the limelight when the 2010 Nobel Prize in Chemistry was awarded for palladium-mediated cross-couplings reactions.<sup>46</sup> A serious drawback of many of these reactions is the use of an expensive and mostly unrecyclable metal catalyst.<sup>47–49</sup> Another setback was the requirement of prefunctionalized coupling partners which was overcome with the activation of C–H bond. The cross-dehydrogenative coupling (CDC) reaction<sup>50</sup> became advantageous for introducing various functional groups. In situations where an oxidant was required, peroxides were used mostly.<sup>51</sup>

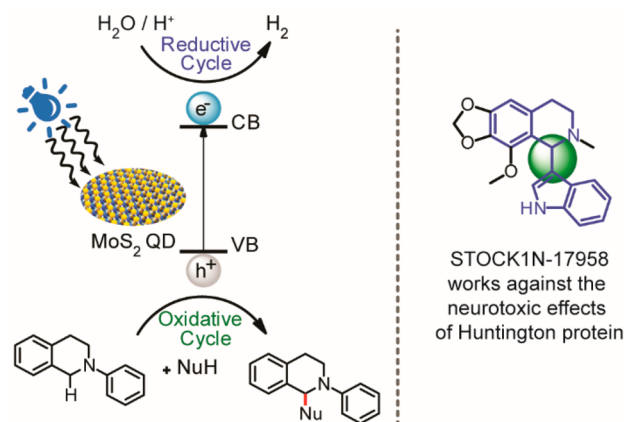
Li et al. developed a protocol to couple activated methylene compounds<sup>52</sup> and other nitroalkanes<sup>53</sup> with tetrahydroisoquinoline using the CuBr/TBHP system, whereas Schnurch et al. carried out the iron-catalyzed indolation of N-protected tetrahydroisoquinolines.<sup>54</sup> CDC reactions resulting in indolation of tetrahydroisoquinoline reported previously mostly required higher temperatures or could also lead to side product(s); for instance, in the CuBr-mediated indolation of tetrahydroisoquinoline, trace amounts of the peroxide product were observed.<sup>55</sup>

Recently, strategies involving the direct transformation of a C–H bond to a C–C bond efficiently without any harsh conditions have been of great interest. In a parallel field, scientists have realized the importance of hydrogen as a renewable and sustainable source of energy. Consequentially, HER has continued to gain momentum in the research community. In a typical photocatalytic HER, sacrificial amine donors are used along with a semiconducting catalyst and a photosensitizer.<sup>56</sup> At the end of the process, the byproduct from the donor amines is rendered useless and the photosensitizer is wasted. We envisioned that the same could be used for a coupling reaction in a milder protocol, using MoS<sub>2</sub> QDs but without the use of any additional photosensitizer. Such a merger of catalysis and HER was reported using an external photosensitizer or based on a photoelectrochemical setup previously.<sup>57–59</sup> In continuation of our efforts for developing better and efficient strategies for transforming C–H bonds to C–C bonds, we now targeted the coupling reaction of N-aryltetrahydroisoquinolines with other nucleophiles using MoS<sub>2</sub> QDs (Scheme 1). N-Aryltetrahydroisoquinolines are important core structures in many pharmaceutical products. 1-Aryltetrahydroisoquinoline analogues are known to possess anti-HIV activity.<sup>60</sup> Indoles are important motifs in biologically relevant molecules,<sup>61</sup> and the coupled analogues such as STOCK1N-17958 are also well-documented in the literature.<sup>62,63</sup> Devising such strategies could open new horizons in synthetic chemistry.

## RESULTS AND DISCUSSION

Following the discussed protocol, MoS<sub>2</sub> QDs were prepared. The biggest challenge in preparing MoS<sub>2</sub> QDs using a bottom-up approach is to prevent the formation/contamination with carbon dots. The prepared material was characterized by

### Scheme 1. Photomediated Oxidation and Reduction Cycle of MoS<sub>2</sub> QDs<sup>a</sup>



<sup>a</sup>The reduction cycle produces H<sub>2</sub> from water, and the oxidative cycle culminates in the CDC product.

various methods before their potential as a catalyst was explored.

Among all of the characterization techniques employed, transmission electron microscopy (TEM) imaging can give concrete evidence of the crystallinity and layered morphology of the material. A dilute solution of the material was drop-casted on a Formvar/carbon 200 mesh copper grid. The *d*-spacing was 0.26 nm, which also confirms that the material is not C-dot (C-dots typically have a *d*-spacing of around 0.21 nm).<sup>64</sup> From the TEM pattern, the size of the dots lies in the range of 6–8 nm. The uniformity is also confirmed by the TEM and a high-resolution TEM (HRTEM) pattern. From the selected area electron diffraction (SAED) pattern, we concluded that the QDs were trigonal prismatic (2H-polymorph or semiconducting type) in nature (Figure 1).

To substantiate the formation of MoS<sub>2</sub> QDs, the UV–visible spectrum was recorded. In a 1 mL quartz cuvette with a 10 mm optical path, the diluted sample was taken and scanned from 200 to 800 nm with a step duration of 0.5 nm. The peak at 264 nm corresponds to MoS<sub>2</sub> QDs (C-dots give a characteristic

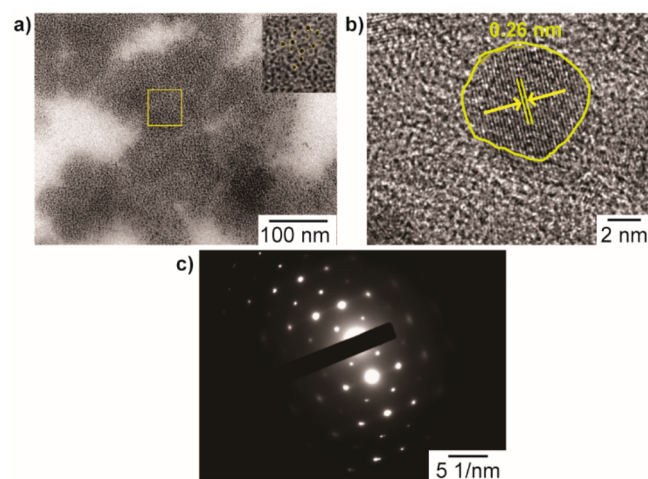


**Figure 1.** TEM characterization of MoS<sub>2</sub> blue QDs: (a) TEM image (inset: magnified image of the area enclosed in the rectangle); (b) HRTEM image; (c) SAED pattern confirming the crystalline nature of the QDs and a trigonal prismatic arrangement of the atoms.

peak above 305 nm; we have observed from the control study done with L-cysteine, subjected to the same conditions excluding the molybdate precursor) (Figure 2a, red line).

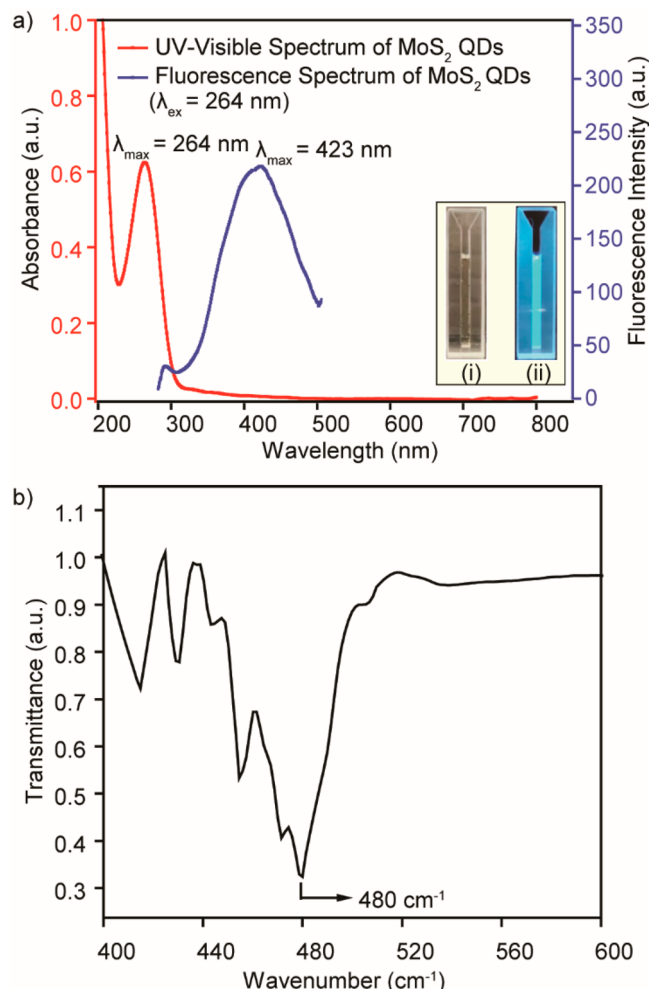


**Figure 2.** (a) UV-visible spectrum (red) and fluorescence spectrum (blue) of MoS<sub>2</sub> blue QDs: the former confirms the absence of a C-dot (inset: naked eye visualization of the as-prepared QDs in (i) white light and (ii) UV light). (b) Fourier transform infrared spectrum showing the Mo-S vibration peak.

From the UV-visible spectrum, we calculated a band gap of 4.7 eV, which is relatively higher than that of C-dots.<sup>65</sup> In contrast, the monolayered 2H-nanosheet possesses a band gap of 1.7–1.9 eV.<sup>66</sup> The increase in band gap for the QDs is an indication of the successful breakdown of dimensionality. The energy levels become discrete consequentially. Upon excitation at 264 nm, the emission spectrum was obtained with the maxima at 423 nm (Figure 2a, blue line). The IR spectrum gave the characteristic Mo-S vibration peak at  $480 \text{ cm}^{-1}$ , confirming the existence of MoS<sub>2</sub> in the material. The spectrum was recorded by dissolving the lyophilized sample in MeOH (Figure 2b).<sup>67</sup>

To obtain the powder X-ray diffraction (PXRD) pattern, the solid material was spread on the glass surface. With bulk MoS<sub>2</sub>, a strong diffraction peak is observed at  $2\theta = 14.4^\circ$ , corresponding to the (002) plane, which generally indicates the presence of a multilayered structure with layer-to-layer interaction. However, as we can see in Figure 3a, no interference peaks are observed, which confirms the formation

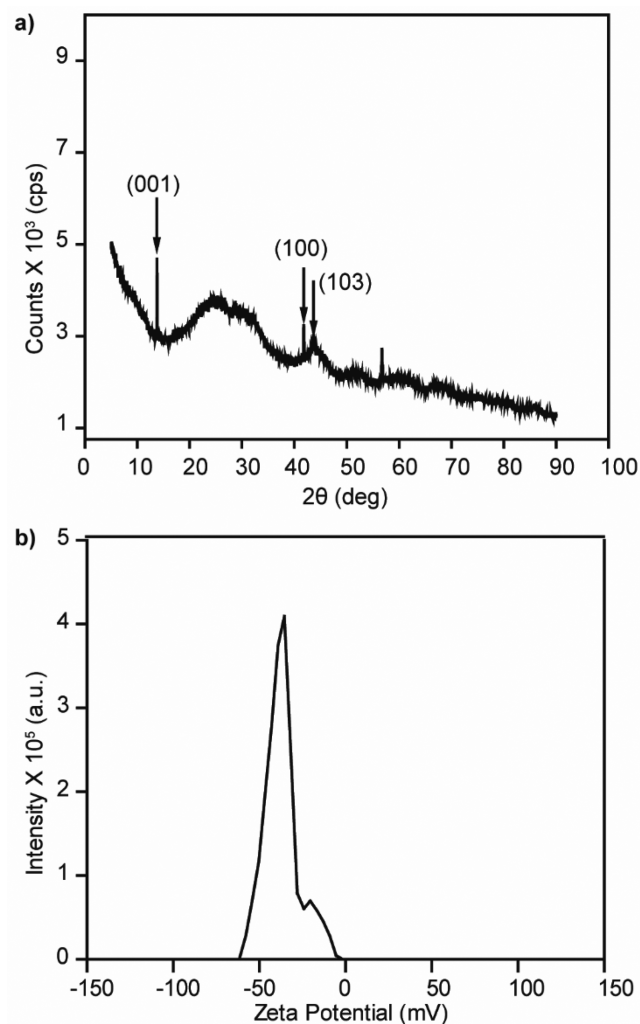


**Figure 3.** (a) PXRD pattern of MoS<sub>2</sub> QDs confirms the presence of discrete layered material and hexagonal arrangement of Mo and S. (b) Zeta-potential measurement explaining the exceptional stability of the MoS<sub>2</sub> QDs solution.

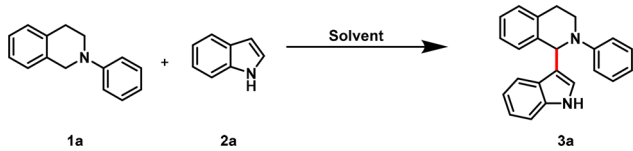
of thin or single-layered material. Additionally, the presence of the assigned planes (001), (100), and (103) corresponding to  $2\theta = 13.85$ ,  $41.86$ , and  $43.57^\circ$ , respectively, reconfirms the presence of hexagonal 2H-MoS<sub>2</sub> (Figure 3a).<sup>3,68</sup> The colloidal stability and nonaggregation nature of these synthesized QDs also can be justified through their surface charge measurement. For that, a zeta-potential measurement was carried out, and a value of  $-39.5 \text{ mV}$  was observed for the QDs. A higher value of zeta-potential for nanomaterials enhances the stability by preventing aggregation (Figure 3b). More significantly, the solution was found to retain stability for over a year with no change in optical and microscopic properties. This was an important advantage of TMD QDs over exfoliated single-layered TMDs. Quantum yield (QY) measurements were carried out using 7-hydroxycoumarin as the reference. The prepared QDs were found to possess a QY of 2.6% (details in section 9 of the Supporting Information (SI)), which is comparable to that of other nanodots.<sup>69</sup>

Following the preparation and characterization of MoS<sub>2</sub> QDs, we proceeded to explore the utility of this semi-conducting nanomaterial for broadly relevant coupling reactions, as stated in the Introduction. We initiated our



study by taking 2-phenyl-1,2,3,4-tetrahydroisoquinoline **1a** with indole **2a** as model substrates (Table 1). We were glad to

Table 1. Optimization of Reaction Conditions<sup>a</sup>



entry	QDs wt % (relative to <b>1a</b> )	oxidant	power (W)	time (h)	solvent	NMR yield (%) <sup>b</sup>
1	1	O <sub>2</sub>	10B	30	H <sub>2</sub> O	63
2	2	O <sub>2</sub>	10B	30	H <sub>2</sub> O	86 (94)
3	3	O <sub>2</sub>	10B	30	H <sub>2</sub> O	50
4	2	O <sub>2</sub>	20B	30	H <sub>2</sub> O	41
5	2	O <sub>2</sub>	45W	30	H <sub>2</sub> O	35
6	2	O <sub>2</sub>	7B	30	H <sub>2</sub> O	32
7	2	O <sub>2</sub>	10B	30	H <sub>2</sub> O: CH <sub>3</sub> CN (4:1)	50
8 <sup>c</sup>		O <sub>2</sub>		30	H <sub>2</sub> O	04
9 <sup>d</sup>	2	O <sub>2</sub>		30	H <sub>2</sub> O	06
10 <sup>e</sup>	2	O <sub>2</sub>		30	H <sub>2</sub> O	06
11 <sup>f</sup>		O <sub>2</sub>	10B	30	H <sub>2</sub> O	28
12	2	Ar	10B	30	H <sub>2</sub> O	20
13		O <sub>2</sub>		30	H <sub>2</sub> O	n.d.

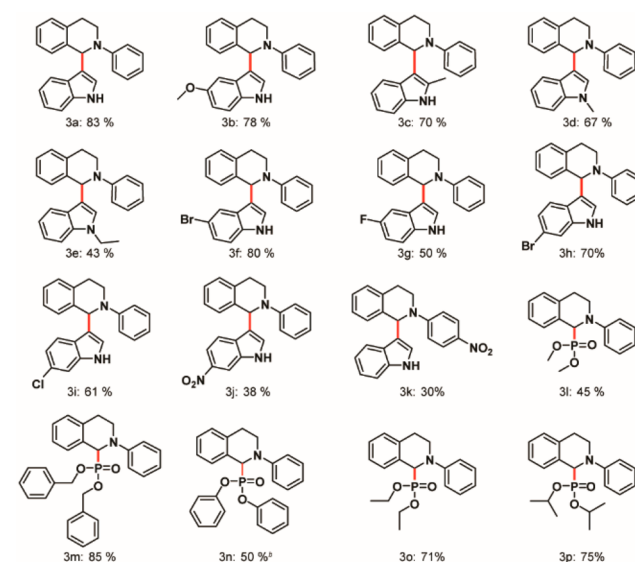
<sup>a</sup>Reaction conditions: 0.1 mmol of 2-phenyl-1,2,3,4-tetrahydroisoquinoline **1a**, 0.25 mmol of indole **2a**, hydrothermally prepared MoS<sub>2</sub> QDs at a strength of 4 mg/mL (except entries 8 and 11) with total volume adjusted to 5 mL with H<sub>2</sub>O (except entry 7); solution was ultrasonicated for dispersing the substrates in the solvent, followed by irradiation with the aforesaid lamp (except entries 8–10) for the mentioned time under O<sub>2</sub> (except entry 12) atmosphere at room temperature (except entries 8 and 9). <sup>b</sup>NMR yields were determined using terephthalaldehyde as reference (number in bracket, if any, indicates % conversion as for entry 2). All reactions were carried out for 30 h (B, blue LED; W, white LED). <sup>c</sup>Heating at 50 °C without light or QDs. <sup>d</sup>Heating at 50 °C without light but with QDs. <sup>e</sup>Without light. <sup>f</sup>Without QDs.

observe the formation of the desired product in the presence of the 1 wt % of MoS<sub>2</sub> QDs, 0.1 mmol of **1a**, and 0.25 mmol **2a** in 5 mL of water. Upon screening various proportions of MoS<sub>2</sub> QDs, we obtained the highest yield at 2 wt % (relative to **1a**) (Table 1, entries 1–3) in water under 10 W blue LED irradiation. The lowering of yield at 3 wt % may be attributed to the aggregation phenomena exhibited by nanomaterials beyond a certain concentration.<sup>70</sup> We tried various other light sources, but each furnished lower yield than a 10 W blue LED (Table 1, entries 4–6). The possible explanation of reduction in yield with an increase in the power of blue LED is the greater collisional quenching of the fluorophores in the latter case. Upon screening a different solvent system, such as acetonitrile (which is the solvent of choice for photoredox transformations), we concluded that water was the optimal solvent for our protocol. Surprisingly, the water–acetonitrile solvent system reduced the yield (Table 1, entry 7) despite being a common choice for many photoredox transformations. The use of water as a solvent was yet another addition to the development of a benign strategy. We now proceeded with the control reactions. First, the above-mentioned reaction does not proceed satisfactorily under thermal conditions solely, hence only a trace amount of product formation was observed with

heating at 50 °C for 30 h (Table 1, entries 8 and 9). To demonstrate the synergistic role of light and QDs, we performed the control experiments in the absence of light and QDs separately. The product formation was significantly less in either case (Table 1, entries 10 and 11). The background reaction can be explained by considering the aerial oxidation of **1a** (Table 1, entry 11). Instead of using H<sub>2</sub>O<sub>2</sub>, we employed O<sub>2</sub> for our reaction to serve as an oxidant. The reaction gave a low yield in the absence of O<sub>2</sub> (Table 1, entry 12). No product formation was observed in the absence of light and QDs at room temperature under an O<sub>2</sub> atmosphere (Table 1, entry 13). In summary, the optimal condition for our protocol was achieved at 2 wt % of QDs in water solvent at room temperature, subjected to an irradiation to a 10 W blue LED for 30 h (Table 1, entry 2).

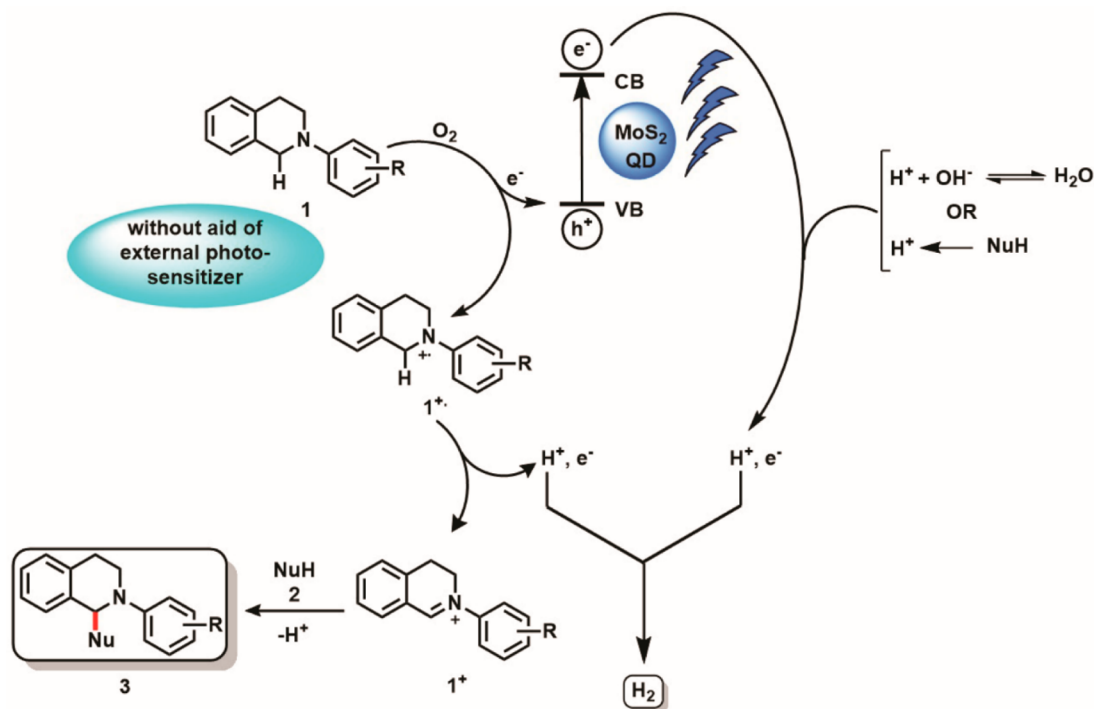
We directed our efforts further to understand the generality of our protocol through substrate scope (Chart 1). No side

Chart 1<sup>a</sup>



<sup>a</sup>Reaction conditions: 0.1 mmol of 2-aryl-1,2,3,4-tetrahydroisoquinoline **1**, 0.25 mmol of indole or phosphite (or its derivative) **2**, 2 wt % (relative to **1**) of hydrothermally prepared MoS<sub>2</sub> QDs at a strength of 4 mg/mL with total volume adjusted to 5 mL with H<sub>2</sub>O or H<sub>2</sub>O/CH<sub>3</sub>CN = 4.5:0.5 (for **3b**, **3c**, **3f–k**); solution was ultrasonicated to disperse the substrates in the solvent, followed by irradiation with a 10 W blue LED for 30 h at room temperature under an O<sub>2</sub> atmosphere. Yields reported are isolated ones except for **3n**. <sup>b</sup>NMR yield was determined using terephthalaldehyde as reference.

product(s) was observed in this developed method (section 5, SI); even in those cases where the yields of the derivatives were low, we could recover the starting material **1a**. A common trend that was observed for substitution on the nitrogen center of indole was a decrease in the yield with increasing crowdedness or sterically demanding substituents on the N-center of indole; that is, the yields followed the trend: R = H > R = Me > R = Et > R = Bn > R = Ph (**3a,d,e** and sections 7.7 and 7.8, SI). Thus, steric effects predominated over inductive or resonance effects. Substitution on the second position of indole with a phenyl moiety gave an unstable product owing to the steric bulkiness (section 7.1, SI), whereas introduction of the methyl moiety gave the target in good yield (**3c**). Substitution on the phenyl ring of indole gave the desired

Scheme 2. Proposed Mechanism for the Catalytic Activity of MoS<sub>2</sub> Blue QDs in CDC Reaction Synchronized with HER

product in moderate to good yields (**3b,f–j**). We further modified the phenyl ring at the N-center of **1a** with a –NO<sub>2</sub> substituent at the para position. The yield was considerably low (**3k**). This observation substantiated the formation of an iminium cation (as illustrated in Scheme 2), which was unstable due to an electron-withdrawing resonance effect of the –NO<sub>2</sub> group, thus explaining the drastic reduction in yield. Various diorganophosphites furnished the desired target in moderate to good yields (**3l–p**), thus elucidating the application of our protocol. We further tried to prepare the starting material with –OMe substitution at the para position. The substrate is unstable during the purification process and decomposes over time at room temperature; hence, we could not proceed in that direction.<sup>71</sup>

The involvement of MoS<sub>2</sub> QDs in the electron transfer process was confirmed by cyclic voltammetry (CV) studies. The ferrocyanide–ferricyanide system (sensitive to the electrode surface) was used with KCl as the electrolyte. The rate of heterogeneous electron transfer (HET) is higher when the anodic–cathodic peak separation ( $\Delta E_p$ ) is narrow, resulting in a better electrocatalytic performance.<sup>72</sup> The voltammogram plot of current versus potential in Figure 4a clearly indicates that the QDs are involved in a HET process. As the peak-to-peak separation decreases in the presence of the material, the reversibility of the process is enhanced in the presence of QDs ( $\Delta E_p$  without QDs = 0.090 V and  $\Delta E_p$  with QDs = 0.077 V).

The recyclability of a nanomaterial is an important aspect with regard to its heterogeneity.<sup>73,74</sup> Ideally, the material should retain its function without appreciable loss of catalytic activity in subsequent runs. We thus examined the reusability of the MoS<sub>2</sub> QDs for the successive cycles of CDC reactions of **1a** with **2a** subjected to the optimized condition. After each run, the reaction mixture was subjected to an ethyl acetate workup, and the aqueous part bearing the nanomaterial was used for the next cycle. The reusability was carried out for up

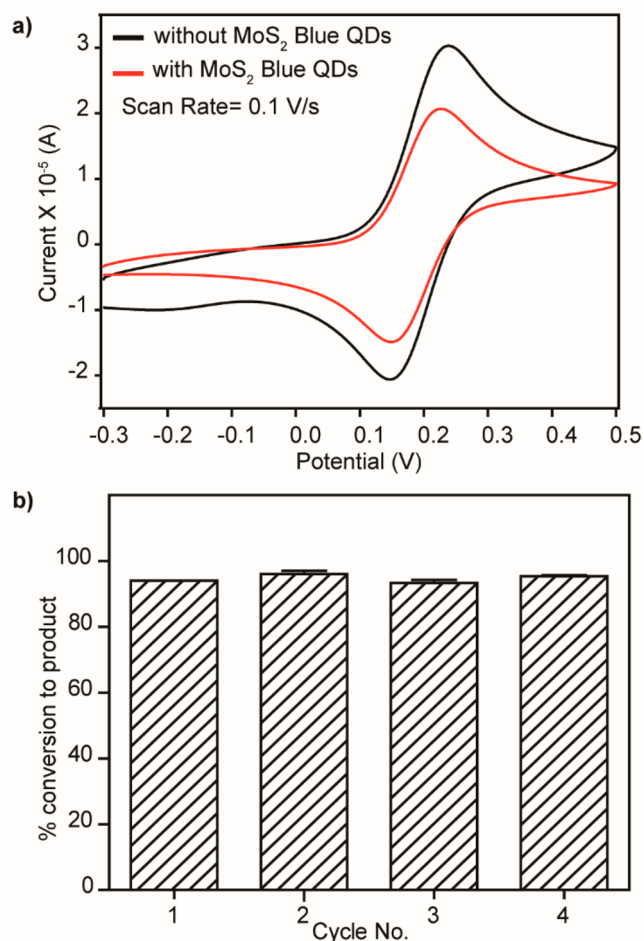


Figure 4. (a) CV studies for HET analysis of hydrothermally prepared MoS<sub>2</sub> QDs. (b) Recyclability of the MoS<sub>2</sub> QDs for the CDC reaction.

to four cycles, and quantitative conversions were obtained. The recyclability test was carried out three times in this way, and the average value was plotted in Figure 4b.

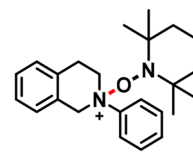
Finally, we studied the scalability of the reaction. When the reaction mixture was scaled up by a factor of 10 (i.e., 1 mmol of **1a**, 2.5 mmol of **2a**, and 2 wt % of MoS<sub>2</sub> QDs in water relative to **1a** irradiated with 10 W blue LED for 30 h), we obtained the desired product in 65% NMR yield.

We were now interested in understanding the mechanism involved in this reaction. Our first target was to determine if a radical propagation mechanism was operative. Thus, we carried out a series of sequential light on–off experiments. If a radical chain pathway governed the process, the reaction would proceed to achieve the yield that we had obtained under the optimal conditions even if the light source was removed after a certain time interval.<sup>75</sup> On the contrary, the yields did not increase when the irradiation was shut down. In other words, the yields up to the time of irradiation and beyond that (until the completion of 30 h) were almost the same. The slight increase was attributed to thermal collision (trace amount of product is formed even in the absence of light; Table 1, entries 8 and 9). Thus, the possibility of a chain mechanism is ruled out (section 6, SI).

We further observed a bathochromic shift in the  $\lambda_{\max}$  of the mixture of MoS<sub>2</sub> QDs and **1a** (at 342 nm) compared to the unmixed components (spectrum recorded in water medium). This supports the fact that the QDs are interacting with **1a** and the resultant bathochromic shift enables them to harvest blue light more efficiently (section 8.a, SI). The emission spectrum of the blue LED used during the experiment was recorded and found to have a broad peak centered around 282 nm, explaining the facile absorption of light (section 8.b, SI). From the visual representation in Figure 2a, it is clear that the material absorbs blue light and emits yellow light.

The decrease in the yields of the reaction upon the use of Na<sub>2</sub>CrO<sub>4</sub> and DIPEA confirms the involvement of electrons and holes in the process (Table 2, entries 1 and 2); the use of

(section 10, SI). Since the step leading to the desired iminium cation **1**<sup>+</sup> is blocked in the presence of TEMPO, the yield decreases.



**1a-TEMP**  
Peak observed in HRMS

Based on these results, we propose a mechanistic pathway for the CDC reaction parallel to the photochemical HER mediated by MoS<sub>2</sub> QDs (Scheme 2). Upon irradiation, an electron is excited to the conduction band (CB) from the valence band (VB). 2-Aryl-1,2,3,4-tetrahydroisoquinoline **1** is oxidized to radical cation **1**<sup>•+</sup> by transferring an electron to the VB to regenerate the ground state of the QD in the presence of O<sub>2</sub>. Any external photosensitizer is not required for the oxidation of **1**. The radical cation of **1** will form the iminium intermediate **1**<sup>+</sup> by losing a H•. The nucleophile **2** attacks the iminium intermediate **1**<sup>+</sup> to give the targeted cross-coupled product **3**. Simultaneously, H<sub>2</sub> evolution occurs as reported in our previous work.<sup>20</sup> Thus, QDs act as a photosensitizer as well as a catalyst and also transfer electron for the water-splitting process. The QDs are further regenerated in the process. In the proposed mechanism, we have stated that the source of H<sub>2</sub> can be from H<sub>2</sub>O as well as the nucleophile NuH. As our target was to design a methodology for the CDC reaction, we did not carry out any deuterated experiments to confirm the source of H<sub>2</sub>. To confirm the source of H<sub>2</sub>, one needs to carry out the experiments with D incorporated at the coupling site of the starting materials, for which the relevant precursor as well as the facility for detection of H<sub>2</sub>/D<sub>2</sub> was beyond our reach.

## CONCLUSION

In conclusion, we have developed an efficient green method based on the use of MoS<sub>2</sub> QDs as the photosensitizer and catalyst for C–C bond formation in the presence of O<sub>2</sub> at room temperature in moderate to good yields under light irradiation. The scope of the protocol is broad, and the material is stable over a prolonged period. Unlike the conventional metal catalysts, our material is recyclable in subsequent runs. No side product has been observed. We hope that the aforesaid strategy paves the way for further developments and innovations in the field of material-mediated catalysis with respect to the fabrication of greener, sustainable, benign, and atom-economical protocols.

## EXPERIMENTAL SECTION

### Preparation of MoS<sub>2</sub> Blue QDs

MoS<sub>2</sub> QDs were prepared using a bottom-up approach reported previously with some required modification.<sup>67</sup> Briefly stated, 0.16 g of Na<sub>2</sub>MoO<sub>4</sub>·2H<sub>2</sub>O was dissolved in 16 mL of H<sub>2</sub>O. The pH of this solution was then adjusted to 6.5 using 0.1 N HCl. In a separate beaker, 0.32 g of L-cysteine was dispersed in 32 mL of H<sub>2</sub>O by ultrasonication. The two solutions were mixed and further transferred to Teflon-lined autoclave chambers. The setup was subjected to a temperature of 200 °C in an autoclave for 36 h. The resulting solution was finally centrifuged at 12,000 rpm for 30 min, and the supernatant was retrieved (schematic illustration in section 4, SI). In the bottom-up approach, slight differences in reaction conditions or even differences in starting concentrations can produce very different

**Table 2. Quenching Experiments<sup>a</sup>**

entry	QDs wt % (relative to <b>1a</b> )	oxidant	power (W)	time (h)	solvent	NMR yield (%) <sup>b</sup>
1 <sup>c</sup>	2	O <sub>2</sub>	10B	30	H <sub>2</sub> O	24
2 <sup>d</sup>	2	O <sub>2</sub>	10B	30	H <sub>2</sub> O	42
3 <sup>e</sup>	2	O <sub>2</sub>	10B	30	H <sub>2</sub> O	28

<sup>a</sup>Reaction conditions: 0.1 mmol of 2-phenyl-1,2,3,4-tetrahydroisoquinoline **1a**, 0.25 mmol of indole **2a**, hydrothermally prepared MoS<sub>2</sub> QDs at a strength of 4 mg/mL with total volume adjusted to 5 mL with H<sub>2</sub>O; solution was ultrasonicated for dispersing the substrates in the solvent, followed by irradiation with a 10 W blue LED (10B) for 30 h at room temperature under O<sub>2</sub> atmosphere. <sup>b</sup>NMR yields were determined using terephthalaldehyde as reference. <sup>c</sup>Na<sub>2</sub>CrO<sub>4</sub> electron scavenger (0.55 mmol). <sup>d</sup>DIPEA hole scavenger (0.1 mmol). <sup>e</sup>TEMPO radical scavenger (0.1 mmol).

TEMPO also resulted in a drastic reduction of the yield (Table 2, entry 3). Na<sub>2</sub>CrO<sub>4</sub> acts as an electron scavenger by blocking the transfer of electrons to the QD from 2-phenyl-1,2,3,4-tetrahydroisoquinoline **1a**. The reaction thus proceeds through the excitation of an electron to the conduction band, generating a hole in the valence band. In the presence of DIPEA, the hole generated in the valence band is quenched. TEMPO reduces the yield by forming the intermediate **1a-TEMP**, the presence of which was confirmed by HRMS



QDs with different defect states; hence, the preparation of the quantum dots was optimized at the initial stages, and the concentrations of all the starting materials as well as subsequent reaction conditions were maintained precisely at every step. In all experimental cycles, we followed the optimized conditions to obtain materials with identical optical and microscopic properties.

The concentration was determined by lyophilization, and the material was characterized spectroscopically (PXRD, UV–visible, and IR spectroscopy) and microscopically (TEM, HRTEM, and SAED).

### General Procedure for the CDC Reaction

After the synthesis and characterization of MoS<sub>2</sub> QDs, its catalytic activity for the cross-dehydrogenative coupling reaction was explored. 2-Phenyl-1,2,3,4-tetrahydroisoquinoline **1a** with indole **2a** was taken in the ratio 1:2.5 in a reaction tube equipped with a magnetic stirring bar. The solution was sonicated to disperse the substrates in the solvent and further subjected to conditions discussed in the optimization table (Table 1). Finally, the reaction mixture was extracted with ethyl acetate (10 mL × 3), dried over anhydrous sodium sulfate, and concentrated by rotary evaporation. The reference was added wherever required to obtain the NMR yield. The crude product was purified on a silica gel (100–200 mesh) column using ethyl acetate/hexane eluent to get the pure product.

For mechanistic investigations, we employed Na<sub>2</sub>CrO<sub>4</sub> as the electron scavenger, DIPEA (*N,N*-diisopropylethylamine) as the hole scavenger, and TEMPO ((2,2,6,6-tetramethylpiperidin-1-yl)oxyl) as the radical scavenger. Specified amounts (discussed in Table 2) of each were added in the reaction mixture, keeping the other optimal conditions intact. After the ethyl acetate workup and concentration of the crude mixture, the effects on the NMR yields were quantified separately with a reference compound.

### Cyclic Voltammetry Study

Ten milliliters of 5 mM [Fe(CN)<sub>6</sub>]<sup>4-</sup> in 0.1 (M) KCl was taken with and without MoS<sub>2</sub> QDs. CV studies were carried out using Pt wire as the counter electrode (cleaned by dipping in concentrated HNO<sub>3</sub> and heating over a burner for a few seconds), glassy carbon electrode as the working electrode, and Ag/AgCl as the reference electrode.

## ■ ASSOCIATED CONTENT

### Supporting Information

The Supporting Information is available free of charge at <https://pubs.acs.org/doi/10.1021/acsorginorgau.1c00040>.

Synthetic protocols, mechanistic study, and characterization data (NMR, HRMS) (PDF)

## ■ AUTHOR INFORMATION

### Corresponding Author

**Mrinmoy De** – Department of Organic Chemistry, Indian Institute of Science, Bangalore, Karnataka 560 012, India; [orcid.org/0000-0001-8394-9059](https://orcid.org/0000-0001-8394-9059); Email: [md@iisc.ac.in](mailto:md@iisc.ac.in)

### Authors

**Komal Jaiswal** – Department of Organic Chemistry, Indian Institute of Science, Bangalore, Karnataka 560 012, India; [orcid.org/0000-0002-6619-697X](https://orcid.org/0000-0002-6619-697X)

**Yarabahally R. Girish** – Centre for Research and Innovation, School of Natural Sciences, Adichunchanagiri University, Mandya 571448, India; [orcid.org/0000-0001-6709-7159](https://orcid.org/0000-0001-6709-7159)

**Pradipta Behera** – Department of Organic Chemistry, Indian Institute of Science, Bangalore, Karnataka 560 012, India

Complete contact information is available at:

<https://pubs.acs.org/10.1021/acsorginorgau.1c00040>

## Author Contributions

The manuscript was written through contributions of all authors. All authors have given approval to the final version of the manuscript.

## Funding

The authors would like to thank SERB CRG/2020/001197 for financial support.

## Notes

The authors declare no competing financial interest.

## ■ ACKNOWLEDGMENTS

The authors wish to express their gratitude to Dr. Aruna Sathyamurthy (Course Instructor, Division of Chemical Sciences, Indian Institute of Science, Bangalore, India) for the CV facility. K.J. thanks PMRF for a doctoral fellowship. P.B. thanks CSIR for a fellowship.

## ■ REFERENCES

- (1) Tian, Z.; Zhang, X.; Li, D.; Zhou, D.; Jing, P.; Shen, D.; Qu, S.; Zboril, R.; Rogach, A. L. Full-Color Inorganic Carbon Dot Phosphors for White-Light-Emitting Diodes. *Adv. Opt. Mater.* **2017**, *5*, 1700416.
- (2) Ding, H.; Wei, J.-S.; Zhang, P.; Zhou, Z.-Y.; Gao, Q.-Y.; Xiong, H.-M. Solvent-Controlled Synthesis of Highly Luminescent Carbon Dots with a Wide Color Gamut and Narrowed Emission Peak Widths. *Small* **2018**, *14*, 1800612.
- (3) Ding, X. G.; Peng, F.; Zhou, J.; Gong, W. B.; Slaven, G.; Loh, K. P.; Lim, C. T.; Leong, D. T. Defect engineered bioactive transition metals dichalcogenides quantum dots. *Nat. Commun.* **2019**, *10*, 41.
- (4) Guo, L.; Ge, J.; Liu, W.; Niu, G.; Jia, Q.; Wang, H.; Wang, P. Tunable multicolor carbon dots prepared from well-defined polythiophene derivatives and their emission mechanism. *Nanoscale* **2016**, *8*, 729–734.
- (5) Ding, H.; Yu, S.-B.; Wei, J.-S.; Xiong, H.-M. Full-Color Light-Emitting Carbon Dots with a Surface-State-Controlled Luminescence Mechanism. *ACS Nano* **2016**, *10*, 484–491.
- (6) Miao, X.; Qu, D.; Yang, D. X.; Nie, B.; Zhao, Y. K.; Fan, H. Y.; Sun, Z. C. Synthesis of Carbon Dots with Multiple Color Emission by Controlled Graphitization and Surface Functionalization. *Adv. Mater.* **2018**, *30*, 1704740.
- (7) Cao, X.; Ding, C.; Zhang, C.; Gu, W.; Yan, Y.; Shi, X.; Xian, Y. Transition metal dichalcogenide quantum dots: synthesis, photoluminescence and biological applications. *J. Mater. Chem. B* **2018**, *6*, 8011–8036.
- (8) Yuan, F.; Wang, Z.; Li, X.; Li, Y.; Tan, Z. a.; Fan, L.; Yang, S. Bright Multicolor Bandgap Fluorescent Carbon Quantum Dots for Electroluminescent Light-Emitting Diodes. *Adv. Mater.* **2017**, *29*, 1604436.
- (9) Bao, L.; Liu, C.; Zhang, Z.-L.; Pang, D.-W. Photoluminescence-Tunable Carbon Nanodots: Surface-State Energy-Gap Tuning. *Adv. Mater.* **2015**, *27*, 1663–1667.
- (10) Hariharan, S.; Karthikeyan, B. Optical and surface band bending mediated fluorescence sensing properties of MoS<sub>2</sub> quantum dots. *RSC Adv.* **2016**, *6*, 101770–101777.
- (11) Ha, H. D.; Han, D. J.; Choi, J. S.; Park, M.; Seo, T. S. Dual Role of Blue Luminescent MoS<sub>2</sub> Quantum Dots in Fluorescence Resonance Energy Transfer Phenomenon. *Small* **2014**, *10*, 3858–3862.
- (12) Ashoori, R. C. Electrons in artificial atoms. *Nature* **1996**, *379*, 413–419.
- (13) Nguyen, T. P.; Sohn, W.; Oh, J. H.; Jang, H. W.; Kim, S. Y. Size-Dependent Properties of Two-Dimensional MoS<sub>2</sub> and WS<sub>2</sub>. *J. Phys. Chem. C* **2016**, *120*, 10078–10085.
- (14) Xu, G. X.; Lin, G. M.; Lin, S. X.; Wu, N.; Deng, Y. Y.; Feng, G.; Chen, Q.; Qu, J. L.; Chen, D. N.; Chen, S. P.; Niu, H. B.; Mei, S. J.; Yong, K. T.; Wang, X. M. The Reproductive Toxicity of CdSe/ZnS

Quantum Dots on the in vivo Ovarian Function and in vitro Fertilization. *Sci. Rep.* **2016**, *6*, 37677.

(15) Hu, L.; Zeng, G.; Chen, G.; Huang, Z.; Wan, J.; Chen, A.; Yu, Z.; Yang, J.; He, K.; Qin, L. Bioaccumulation and toxicity of CdSe/ZnS quantum dots in *Phanerochaete chrysosporium*. *Colloids Surf., B* **2017**, *159*, 303–311.

(16) Chakraborty, I. N.; Roy, S.; Devatha, G.; Rao, A.; Pillai, P. P. InP/ZnS Quantum Dots as Efficient Visible-Light Photocatalysts for Redox and Carbon–Carbon Coupling Reactions. *Chem. Mater.* **2019**, *31*, 2258–2262.

(17) Chandrashekar, H. B.; Maji, A.; Halder, G.; Banerjee, S.; Bhattacharyya, S.; Maiti, D. Photocatalyzed borylation using water-soluble quantum dots. *Chem. Commun.* **2019**, *55*, 6201–6204.

(18) Jaiswal, K.; Girish, Y. R.; De, M. Influence of a Tunable Band Gap on Photoredox Catalysis by Various Two-Dimensional Transition-Metal Dichalcogenides. *ACS Appl. Nano Mater.* **2020**, *3*, 84–93.

(19) Vancso, P.; Popov, Z. I.; Peto, J.; Ollar, T.; Dobrik, G.; Pap, J. S.; Hwang, C. Y.; Sorokin, P. B.; Tapasztó, L. Transition Metal Chalcogenide Single Layers as an Active Platform for Single-Atom Catalysis. *ACS Energy Lett.* **2019**, *4*, 1947–1953.

(20) Girish, Y. R.; Jaiswal, K.; Prakash, P.; De, M. 2D-MoS<sub>2</sub> photocatalyzed cross dehydrogenative coupling reaction synchronized with hydrogen evolution reaction. *Catal. Sci. Technol.* **2019**, *9*, 1201–1207.

(21) Yasaei, P.; Murthy, A. A.; Xu, Y. B.; dos Reis, R.; Shekhawat, G. S.; Dravid, V. P. Spatial Mapping of Hot-Spots at Lateral Heterogeneities in Monolayer Transition Metal Dichalcogenides. *Adv. Mater.* **2019**, *31*, 1808244.

(22) Karunakaran, S.; Pandit, S.; Basu, B.; De, M. Simultaneous Exfoliation and Functionalization of 2H-MoS<sub>2</sub> by Thiolated Surfactants: Applications in Enhanced Antibacterial Activity. *J. Am. Chem. Soc.* **2018**, *140*, 12634–12644.

(23) Maitra, U.; Gupta, U.; De, M.; Datta, R.; Govindaraj, A.; Rao, C. N. Highly effective visible-light-induced H<sub>2</sub> generation by single-layer 1T-MoS<sub>2</sub> and a nanocomposite of few-layer 2H-MoS<sub>2</sub> with heavily nitrogenated graphene. *Angew. Chem., Int. Ed.* **2013**, *52*, 13057–13061.

(24) Li, Y.; Majewski, M. B.; Islam, S. M.; Hao, S.; Murthy, A. A.; DiStefano, J. G.; Hanson, E. D.; Xu, Y.; Wolverson, C.; Kanatzidis, M. G.; Wasielewski, M. R.; Chen, X.; Dravid, V. P. Morphological Engineering of Winged Au@MoS<sub>2</sub> Heterostructures for Electrocatalytic Hydrogen Evolution. *Nano Lett.* **2018**, *18*, 7104–7110.

(25) Chou, S. S.; Sai, N.; Lu, P.; Coker, E. N.; Liu, S.; Artyushkova, K.; Luk, T. S.; Kaehr, B.; Brinker, C. J. Understanding catalysis in a multiphase two-dimensional transition metal dichalcogenide. *Nat. Commun.* **2015**, *6*, 8311.

(26) Tian, X.; Sun, Y. R.; Fan, S. H.; Boudreau, M. D.; Chen, C. Y.; Ge, C. C.; Yin, J. J. Photogenerated Charge Carriers in Molybdenum Disulfide Quantum Dots with Enhanced Antibacterial Activity. *ACS Appl. Mater. Interfaces* **2019**, *11*, 4858–4866.

(27) Zhang, S.; Liu, X.; Liu, C.; Luo, S.; Wang, L.; Cai, T.; Zeng, Y.; Yuan, J.; Dong, W.; Pei, Y.; Liu, Y. MoS<sub>2</sub> Quantum Dot Growth Induced by S Vacancies in a ZnIn<sub>2</sub>S<sub>4</sub> Monolayer: Atomic-Level Heterostructure for Photocatalytic Hydrogen Production. *ACS Nano* **2018**, *12*, 751–758.

(28) Qiao, W.; Yan, S.; Song, X.; Zhang, X.; Sun, Y.; Chen, X.; Zhong, W.; Du, Y. Monolayer MoS<sub>2</sub> quantum dots as catalysts for efficient hydrogen evolution. *RSC Adv.* **2015**, *5*, 97696–97701.

(29) Najafi, L.; Bellani, S.; Martin-Garcia, B.; Oropesa-Nunez, R.; Del Rio Castillo, A. E.; Prato, M.; Moreels, I.; Bonaccorso, F. Solution-Processed Hybrid Graphene Flake/2H-MoS<sub>2</sub> Quantum Dot Heterostructures for Efficient Electrochemical Hydrogen Evolution. *Chem. Mater.* **2017**, *29*, 5782–5786.

(30) Bayat, A.; Zirak, M.; Saievar-Iranizad, E. Vertically Aligned MoS<sub>2</sub> Quantum Dots/Nanoflakes Heterostructure: Facile Deposition with Excellent Performance toward Hydrogen Evolution Reaction. *ACS Sustainable Chem. Eng.* **2018**, *6*, 8374–8382.

(31) Mohanty, B.; Ghorbani-Asl, M.; Kretschmer, S.; Ghosh, A.; Guha, P.; Panda, S. K.; Jena, B.; Krashenninnikov, A. V.; Jena, B. K. MoS<sub>2</sub> Quantum Dots as Efficient Catalyst Materials for the Oxygen Evolution Reaction. *ACS Catal.* **2018**, *8*, 1683–1689.

(32) Lin, H. H.; Wang, C. X.; Wu, J. P.; Xu, Z. Z.; Huang, Y. J.; Zhang, C. Colloidal synthesis of MoS<sub>2</sub> quantum dots: size-dependent tunable photoluminescence and bioimaging. *New J. Chem.* **2015**, *39*, 8492–8497.

(33) Gu, W.; Yan, Y.; Cao, X.; Zhang, C.; Ding, C.; Xian, Y. A facile and one-step ethanol-thermal synthesis of MoS<sub>2</sub> quantum dots for two-photon fluorescence imaging. *J. Mater. Chem. B* **2016**, *4*, 27–31.

(34) Dong, H.; Tang, S.; Hao, Y.; Yu, H.; Dai, W.; Zhao, G.; Cao, Y.; Lu, H.; Zhang, X.; Ju, H. Fluorescent MoS<sub>2</sub> Quantum Dots: Ultrasonic Preparation, Up-Conversion and Down-Conversion Bioimaging, and Photodynamic Therapy. *ACS Appl. Mater. Interfaces* **2016**, *8*, 3107–3114.

(35) Sweet, C.; Pramanik, A.; Jones, S.; Ray, P. C. Two-Photon Fluorescent Molybdenum Disulfide Dots for Targeted Prostate Cancer Imaging in the Biological II Window. *ACS Omega* **2017**, *2*, 1826–1835.

(36) Li, P. S.; Liu, L.; Lu, Q. L.; Yang, S.; Yang, L. F.; Cheng, Y.; Wang, Y. D.; Wang, S. Y.; Song, Y. L.; Tan, F. P.; Li, N. Ultrasmall MoS<sub>2</sub> Nanodots-Doped Biodegradable SiO<sub>2</sub> Nanoparticles for Clearable FL/CT/MSOT Imaging-Guided PTT/PDT Combination Tumor Therapy. *ACS Appl. Mater. Interfaces* **2019**, *11*, 5771–5781.

(37) Chen, L.; Hsieh, S.-L.; Kuo, C.-H.; Hsieh, S.; Chen, W.-H.; Chen, C.-W.; Dong, C.-D. Novel MoS<sub>2</sub> quantum dots as a highly efficient visible-light driven photocatalyst in water remediation. *RSC Adv.* **2020**, *10*, 31794–31799.

(38) Xin, X.; Zhang, Y.; Guan, X. X.; Cao, J. X.; Li, W. L.; Long, X.; Tan, X. Enhanced Performances of PbS Quantum-Dots-Modified MoS<sub>2</sub> Composite for NO<sub>2</sub> Detection at Room Temperature. *ACS Appl. Mater. Interfaces* **2019**, *11*, 9438–9447.

(39) Gu, W.; Yan, Y.; Zhang, C.; Ding, C.; Xian, Y. One-Step Synthesis of Water-Soluble MoS<sub>2</sub> Quantum Dots via a Hydrothermal Method as a Fluorescent Probe for Hyaluronidase Detection. *ACS Appl. Mater. Interfaces* **2016**, *8*, 11272–11279.

(40) Zhu, H.; Zhang, H.; Xia, Y. S. Planar Is Better: Monodisperse Three-Layered MoS<sub>2</sub> Quantum Dots as Fluorescent Reporters for 2,4,6-Trinitrotoluene Sensing in Environmental Water and Luggage Cases. *Anal. Chem.* **2018**, *90*, 3942–3949.

(41) Xia, W.; Zhang, P.; Fu, W.; Hu, L.; Wang, Y. Aggregation/dispersion-mediated peroxidase-like activity of MoS<sub>2</sub> quantum dots for colorimetric pyrophosphate detection. *Chem. Commun.* **2019**, *55*, 2039–2042.

(42) Wang, J.; Tan, X.; Pang, X.; Liu, L.; Tan, F.; Li, N. MoS<sub>2</sub> Quantum Dot@Polyaniline Inorganic-Organic Nanohybrids for in Vivo Dual-Modal Imaging Guided Synergistic Photothermal/Radiation Therapy. *ACS Appl. Mater. Interfaces* **2016**, *8*, 24331–24338.

(43) Yadav, V.; Roy, S.; Singh, P.; Khan, Z.; Jaiswal, A. 2D MoS<sub>2</sub>-Based Nanomaterials for Therapeutic, Bioimaging, and Biosensing Applications. *Small* **2019**, *15*, 1803706.

(44) Arul, N. S.; Nithya, V. D. Molybdenum disulfide quantum dots: synthesis and applications. *RSC Adv.* **2016**, *6*, 65670–65682.

(45) Johansson Seechurn, C. C. C.; Kitching, M. O.; Colacot, T. J.; Snieckus, V. Palladium-Catalyzed Cross-Coupling: A Historical Contextual Perspective to the 2010 Nobel Prize. *Angew. Chem., Int. Ed.* **2012**, *51*, 5062–5085.

(46) Colacot, T. J. The 2010 Nobel Prize in Chemistry: Palladium-Catalyzed Cross-Coupling. *Platinum Met. Rev.* **2011**, *55*, 84–90.

(47) Murahashi, S.; Nakae, T.; Terai, H.; Komiya, N. Ruthenium-catalyzed oxidative cyanation of tertiary amines with molecular oxygen or hydrogen peroxide and sodium cyanide: sp<sup>3</sup> C-H bond activation and carbon-carbon bond formation. *J. Am. Chem. Soc.* **2008**, *130*, 11005–11012.

(48) Bartling, H.; Eisenhofer, A.; König, B.; Gschwind, R. M. The Photocatalyzed Aza-Henry Reaction of *N*-Aryltetrahydroisoquino-



lines: Comprehensive Mechanism, H<sup>-</sup> versus H<sup>+</sup>-Abstraction, and Background Reactions. *J. Am. Chem. Soc.* **2016**, *138*, 11860–11871.

(49) Wu, Y. C.; Peng, X. P.; Luo, B. L.; Wu, F. H.; Liu, B.; Song, F. Y.; Huang, P.; Wen, S. J. Palladium catalyzed dual C-H functionalization of indoles with cyclic diaryliodoniums, an approach to ring fused carbazole derivatives. *Org. Biomol. Chem.* **2014**, *12*, 9777–9780.

(50) Li, C. J. Cross-dehydrogenative coupling (CDC): exploring C-C bond formations beyond functional group transformations. *Acc. Chem. Res.* **2009**, *42*, 335–344.

(51) Groll, B.; Schaaf, P.; Mihovilovic, M. D.; Schnurch, M. Cu(I)-catalyzed one-pot decarboxylation-alkynylation reactions on 1,2,3,4-tetrahydroisoquinolines and one-pot synthesis of triazolyl-1,2,3,4-tetrahydroisoquinolines. *J. Mol. Catal. A: Chem.* **2017**, *426*, 398–406.

(52) Li, Z. P.; Li, C. J. Highly efficient CuBr-catalyzed cross-dehydrogenative coupling (CDC) between tetrahydroisoquinolines and activated methylene compounds. *Eur. J. Org. Chem.* **2005**, *2005*, 3173–3176.

(53) Li, Z.; Li, C. J. Highly efficient copper-catalyzed nitro-Mannich type reaction: cross-dehydrogenative-coupling between sp<sup>3</sup> C-H bond and sp<sup>3</sup> C-H bond. *J. Am. Chem. Soc.* **2005**, *127*, 3672–3673.

(54) Ghobrial, M.; Harhammer, K.; Mihovilovic, M. D.; Schnurch, M. Facile, solvent and ligand free iron catalyzed direct functionalization of N-protected tetrahydroisoquinolines and isochroman. *Chem. Commun. (Cambridge, U. K.)* **2009**, *46*, 8836–8838.

(55) Li, Z.; Li, C. J. CuBr-catalyzed direct indolation of tetrahydroisoquinolines via cross-dehydrogenative coupling between sp<sup>3</sup> C-H and sp<sup>2</sup> C-H bonds. *J. Am. Chem. Soc.* **2005**, *127*, 6968–6969.

(56) Chou, S. S.; Sai, N.; Lu, P.; Coker, E. N.; Liu, S.; Artyushkova, K.; Luk, T. S.; Kaehr, B.; Brinker, C. J. Understanding catalysis in a multiphase two-dimensional transition metal dichalcogenide. *Nat. Commun.* **2015**, *6*, 8311.

(57) Chen, B.; Wu, L.-Z.; Tung, C.-H. Photocatalytic Activation of Less Reactive Bonds and Their Functionalization via Hydrogen-Evolution Cross-Couplings. *Acc. Chem. Res.* **2018**, *51*, 2512–2523.

(58) Meng, Q.-Y.; Zhong, J.-J.; Liu, Q.; Gao, X.-W.; Zhang, H.-H.; Lei, T.; Li, Z.-J.; Feng, K.; Chen, B.; Tung, C.-H.; Wu, L.-Z. A Cascade Cross-Coupling Hydrogen Evolution Reaction by Visible Light Catalysis. *J. Am. Chem. Soc.* **2013**, *135*, 19052–19055.

(59) Wang, J.-H.; Li, X.-B.; Li, J.; Lei, T.; Wu, H.-L.; Nan, X.-L.; Tung, C.-H.; Wu, L.-Z. Photoelectrochemical cell for P-H/C-H cross-coupling with hydrogen evolution. *Chem. Commun.* **2019**, *55*, 10376–10379.

(60) Cheng, P.; Huang, N.; Jiang, Z. Y.; Zhang, Q.; Zheng, Y. T.; Chen, J. J.; Zhang, X. M.; Ma, Y. B. 1-aryl-tetrahydroisoquinoline analogs as active anti-HIV agents in vitro. *Bioorg. Med. Chem. Lett.* **2008**, *18*, 2475–2478.

(61) Somei, M.; Yamada, F. Simple indole alkaloids and those with a non-rearranged monoterpene unit. *Nat. Prod. Rep.* **2005**, *22*, 73–103.

(62) Bentley, K. W.  $\beta$ -Phenylethylamines and the isoquinoline alkaloids. *Nat. Prod. Rep.* **2004**, *21*, 395–424.

(63) Stockwell, B.; Hoffstrom, B.; Varma, H. Agents For Treating Neurodegenerative Diseases. Patent No. WO 2008016659A2 (Google Patents), 2007.

(64) Jiang, L. F.; Zeng, H. B. Comment on “Strongly luminescent monolayered MoS<sub>2</sub> prepared by effective ultrasound exfoliation. *Nanoscale* **2013**, *5*, 4580; *Nanoscale* **2015**, *7*, 4580–4583.

(65) Yu, P.; Wen, X.; Toh, Y.-R.; Tang, J. Temperature-Dependent Fluorescence in Carbon Dots. *J. Phys. Chem. C* **2012**, *116*, 25552–25557.

(66) Kang, M.; Kim, B.; Ryu, S. H.; Jung, S. W.; Kim, J.; Moreschini, L.; Jozwiak, C.; Rotenberg, E.; Bostwick, A.; Kim, K. S. Universal Mechanism of Band-Gap Engineering in Transition-Metal Dichalcogenides. *Nano Lett.* **2017**, *17*, 1610–1615.

(67) Wang, Y.; Ni, Y. N. Molybdenum Disulfide Quantum Dots as a Photoluminescence Sensing Platform for 2,4,6-Trinitrophenol Detection. *Anal. Chem.* **2014**, *86*, 7463–7470.

(68) Xu, S.; Li, D.; Wu, P. One-Pot, Facile, and Versatile Synthesis of Monolayer MoS<sub>2</sub>/WS<sub>2</sub> Quantum Dots as Bioimaging Probes and Efficient Electrocatalysts for Hydrogen Evolution Reaction. *Adv. Funct. Mater.* **2015**, *25*, 1127–1136.

(69) Baker, D. R.; Kamat, P. V. Tuning the Emission of CdSe Quantum Dots by Controlled Trap Enhancement. *Langmuir* **2010**, *26*, 11272–11276.

(70) Noh, M.; Kim, T.; Lee, H.; Kim, C.-K.; Joo, S.-W.; Lee, K. Fluorescence quenching caused by aggregation of water-soluble CdSe quantum dots. *Colloids Surf., A* **2010**, *359*, 39–44.

(71) Nauth, A. M.; Otto, N.; Opatz, T.  $\alpha$ -Cyanation of Aromatic Tertiary Amines using Ferricyanide as a Non-Toxic Cyanide Source. *Adv. Synth. Catal.* **2015**, *357*, 3424–3428.

(72) Rohaizad, N.; Mayorga-Martinez, C. C.; Sofer, Z.; Pumera, M. 1T-Phase Transition Metal Dichalcogenides (MoS<sub>2</sub>, MoSe<sub>2</sub>, WS<sub>2</sub>, and WSe<sub>2</sub>) with Fast Heterogeneous Electron Transfer: Application on Second-Generation Enzyme-Based Biosensor. *ACS Appl. Mater. Interfaces* **2017**, *9*, 40697–40706.

(73) Kumar, S.; T, S.; Kumar, B.; Baruah, A.; Shanker, V. Synthesis of Magnetically Separable and Recyclable g-C<sub>3</sub>N<sub>4</sub>-Fe<sub>3</sub>O<sub>4</sub> Hybrid Nanocomposites with Enhanced Photocatalytic Performance under Visible-Light Irradiation. *J. Phys. Chem. C* **2013**, *117*, 26135–26143.

(74) Liu, W.; Cai, J.; Li, Z. Self-Assembly of Semiconductor Nanoparticles/Reduced Graphene Oxide (RGO) Composite Aerogels for Enhanced Photocatalytic Performance and Facile Recycling in Aqueous Photocatalysis. *ACS Sustainable Chem. Eng.* **2015**, *3*, 277–282.

(75) Xu, Z.-M.; Li, H.-X.; Young, D. J.; Zhu, D.-L.; Li, H.-Y.; Lang, J.-P. Exogenous Photosensitizer-, Metal-, and Base-Free Visible-Light-Promoted C-H Thiolation via Reverse Hydrogen Atom Transfer. *Org. Lett.* **2019**, *21*, 237–241.